Mid-infrared electroluminescence from InAs type-I quantum wells grown on InAsP/InP metamorphic buffers

Daehwan Jung, Lan Yu, Daniel Wasserman, and Minjoo Larry Lee

Citation: Journal of Applied Physics **118**, 183101 (2015); doi: 10.1063/1.4935418
View online: http://dx.doi.org/10.1063/1.4935418
View Table of Contents: http://scitation.aip.org/content/aip/journal/jap/118/18?ver=pdfcov
Published by the AIP Publishing

JOURNAL OF APPLIED PHYSICS **118**, 183101 (2015)

Mid-infrared electroluminescence from InAs type-I quantum wells grown on InAsP/InP metamorphic buffers

Daehwan Jung,[1,a)] Lan Yu,[2] Daniel Wasserman,[2] and Minjoo Larry Lee[1]
[1]*Department of Electrical Engineering, Yale University, New Haven, Connecticut 06520, USA*
[2]*Department of Electrical and Computer Engineering, University of Illinois at Urbana-Champaign, Urbana, Illinois 61801, USA*

(Received 14 August 2015; accepted 28 October 2015; published online 9 November 2015)

We report room-temperature (RT) electroluminescence (EL) from InAs/$InAs_xP_{1-x}$ quantum well (QW) light-emitting diodes (LEDs) over a wide wavelength range of 2.50–2.94 μm. We demonstrate the ability to accurately design strained InAs QW emission wavelengths while maintaining low threading dislocation density, coherent QW interfaces, and high EL intensity. Investigation of the optical properties of the LEDs grown on different $InAs_xP_{1-x}$ metamorphic buffers showed higher EL intensity and lower thermal quenching for QWs with higher barriers and stronger carrier confinement. Strong RT EL intensity from LEDs with narrow full-width at half-maximum shows future potential for InAs QW mid-infrared laser diodes on InAsP/InP. © *2015 AIP Publishing LLC*. [http://dx.doi.org/10.1063/1.4935418]

I. INTRODUCTION

Mid-infrared (mid-IR) lasers emitting around $\lambda = 2$–$8\ \mu$m have important applications such as molecular spectroscopy and gas detection.[1] GaSb-based type-I quantum well (QW) laser diodes can cover most of the short mid-IR spectral range ($\lambda = 1.9$–$3.7\ \mu$m) at room temperature (RT) under continuous wave (CW) operation, enabled by the recent improvement in hole confinement afforded by the AlGaInAsSb quinary system.[2,3] Also, interband cascade lasers employing type-II active regions on GaSb have shown RT CW lasing at $\lambda = 3.0$–$5.5\ \mu$m with relatively low threshold current densities.[4]

However, compared to GaSb substrates, InP substrates offer significant advantages, including more mature commercial processing infrastructure and higher thermal conductivity. For conventional type-I laser diodes on InP, Sato *et al.* demonstrated RT CW emission at 2.33 μm using highly strained InAs/InGaAs QWs,[5] and recently Gu *et al.* demonstrated 2.37 μm laser diodes by employing triangular InAs QWs to lower the type-I transition energy.[6] However, the InAs QW critical thickness constraint limits further increases in type-I QW emission wavelength on the InP lattice constant. As an alternative, InGaAs/GaAsSb type-II structures have been employed on InP, and recently Sprengel *et al.* demonstrated type-II laser diodes at 2.6 μm in pulsed mode at RT and at 2.3 μm in the CW mode at 0 °C.[7] On the longer wavelength side for InP-based technologies, quantum cascade lasers (QCLs) have recently achieved significant advances with high output power and RT CW lasing at $\lambda = 3.0\ \mu$m.[8] Even with the merits of high power output under RT CW operation, QCLs fundamentally require high turn-on voltages (~12 V) and large threshold currents, leading to high threshold power densities. Furthermore, to emit wavelengths close to 3 μm, highly strained InGaAs/InAlAs growth is required for large conduction band offsets. This leads to even higher turn-on voltages (~18 V) and a decrease in wall-plug-efficiency (WPE) to 0.031% for RT CW operation;[9] in contrast, type-I laser diodes on GaSb emitting at 3.0 μm show 8.8% WPE with ~1.4 V for RT CW operation.[2] The realization of efficient RT CW InP-based lasers for $\lambda = 2.4$–$3.0\ \mu$m will be highly challenging due to the very high strain in both conventional type-I laser diodes and QCLs.

Compositionally graded metamorphic buffers such as $In_xAl_{1-x}As$ or $InAs_xP_{1-x}$ enable type-I technology on InP to overcome the InAs QW critical thickness limit and to extend the operational wavelengths of InP-based lasers beyond 2.37 μm. Recently, Gu *et al.* showed metamorphic mid-IR laser diodes emitting at 2.9 μm from type-I InAs QWs using $In_xAl_{1-x}As$/InP graded buffers.[10,11] However, CW lasing persisted up to only 180 K, and considerable spontaneous emission from the InGaAs waveguide was observed due to unfavorable carrier confinement in their active region. Alternatively, mixed anion $InAs_xP_{1-x}$ buffers may serve as a better platform for metamorphic mid-IR light emitters than $In_xAl_{1-x}As$ buffers because of their lower threading dislocation density (TDD), lower surface roughness, and lack of phase separation.[12] Previously, we reported 2.8 μm RT photoluminescence (PL) emission from type-I $InAs_{0.94}P_{0.06}$/$InAs_{0.78}P_{0.22}$ MQWs grown on $InAs_xP_{1-x}$ buffers that showed potential for mid-IR light-emitters.[13]

In this work, we demonstrate RT electroluminescence (EL) at $\lambda = 2.50$–$2.94\ \mu$m from InP-based light-emitting diodes (LEDs) using strained InAs/$InAs_xP_{1-x}$ QWs. Engineering of the InAs QW thickness and $InAs_xP_{1-x}$ barrier composition enabled us to achieve precise wavelength tuning of the metamorphic LEDs while maintaining TDDs of 2–$5 \times 10^6\ cm^{-2}$ and smooth, coherent interfaces between the QW and barriers. Also, we found that LEDs emitting at 2.50 μm demonstrated higher EL intensity and lower thermal quenching than devices emitting at 2.94 μm. The measured

a)daehwan.jung@yale.edu

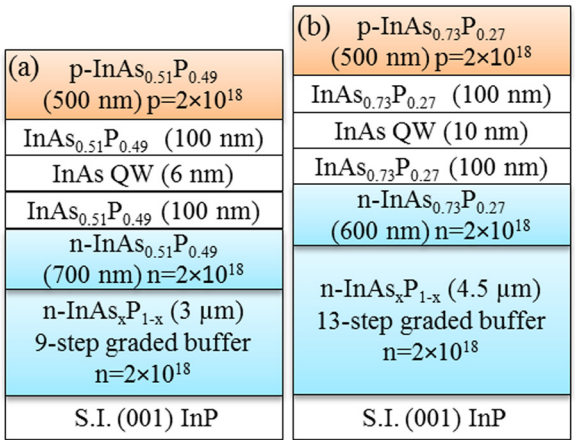

FIG. 1. Cross-sectional schematics of (a) sample A and (b) sample B. The buffer thicknesses were designed to have a grading rate of ~0.5%/μm in both samples.

EL peak energies from both samples closely match calculated QW transition energies from 77 K to 300 K using a valence band offset $\Delta E_v = 0.35\Delta E_g$. Strong RT EL intensities with small full-width at half-maxima (FWHM) are encouraging for future InP-based metamorphic InAs/$InAs_xP_{1-x}$ type-I QW laser diodes.

II. EXPERIMENTAL DETAILS

LED samples were grown on semi-insulating (001) InP substrates in a Veeco Mod Gen-II solid source molecular beam epitaxy system. Figure 1 shows the cross-sectional schematics of the two LED structures (samples A and B) investigated in this work. We first grew metamorphic $InAs_xP_{1-x}$ step-graded buffers by fixing the P_2 flux while increasing the As_2 flux. V/III beam equivalent pressure ratios increased from 10.8 to 13.3 for sample A and from 10.8 to 16.8 for sample B; the growth rate was 1 μm/h for all layers. The step size of both buffers is 300 nm, except for the 5th layer in sample A and the 4th and 8th layers in sample B, which are doubled in thickness and serve as x-ray diffraction marker layers. The buffers and caps were doped using Si for n-type and Be for p-type, respectively, both at a nominal concentration of 2×10^{18} cm^{-3}. To minimize P-incorporation into the InAs QW, a growth interruption occurred prior to initiation of QW growth under As_2 overpressure for 1 min to pump out the remaining P_2 in the chamber.

The growth temperature for the $InAs_xP_{1-x}$ buffers was 470 °C, as measured by optical pyrometer, to ensure high dislocation glide velocity during the strain relaxation process[14] as well as to maintain smooth surface morphology. *In situ* reflection high-energy electron diffraction (RHEED) showed streaky (2×4) patterns throughout the buffer growth as shown in Figure 2(a), while the optical microscope image of Figure 2(b) reveals smooth surface morphology with the expected cross-hatch pattern; atomic force microscopy (not shown) gave root mean square (RMS) surface roughness values of 2–4 nm.

Several test samples were grown at a slightly higher temperature of 495 °C in an attempt to enhance dislocation glide velocity. However, the RHEED pattern for the $InAs_xP_{1-x}$ buffers grown at 495 °C transitioned to (4×4) at $x \sim 0.25$ [Fig. 2(c)], which may indicate the coexistence of (2×4) and (4×2) domains on the surface. All such samples showed extremely rough surface morphology [Fig. 2(d)], which is consistent with earlier observations that the InAs

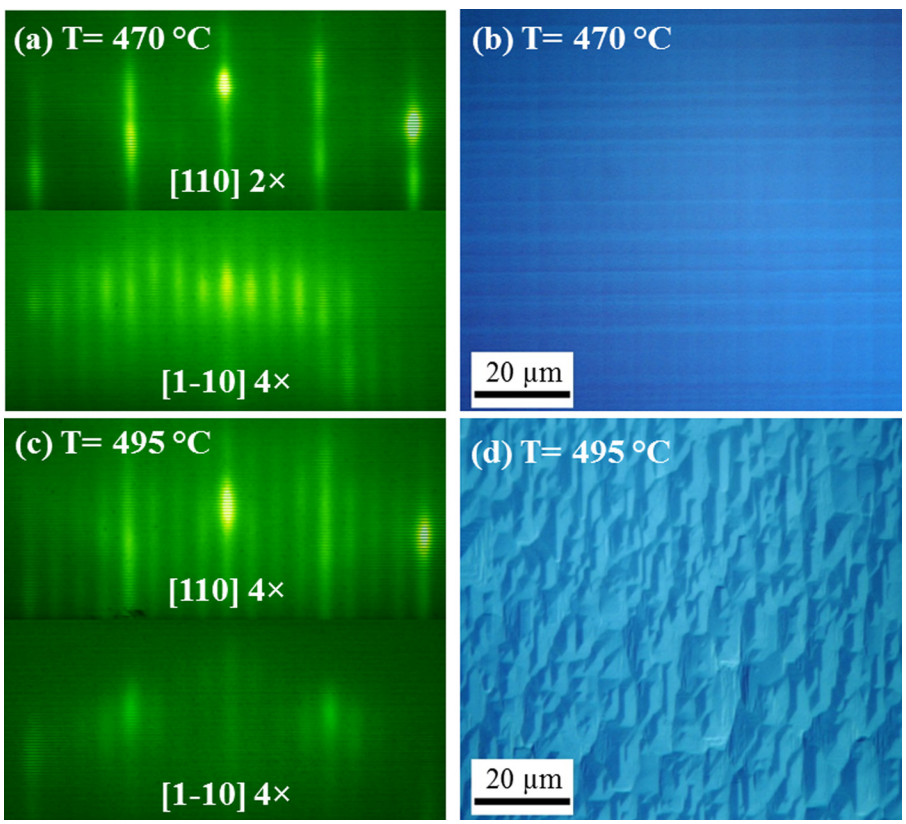

FIG. 2. (a) (2×4) RHEED pattern during InAsP buffer growth at 470 °C and (b) optical microscope image showing cross-hatched surface. (c) (4×4) RHEED pattern during InAsP buffer growth at 495 °C and (d) optical microscope image showing rough surface.

(4×2) growth regime leads to a high density of microscale pyramid defects and high RMS roughness.[15–17] The specific RHEED transition temperatures are expected to depend sensitively on the $InAs_xP_{1-x}$ composition, V/III ratio, and method of temperature measurement. However, these results show the importance of staying within a (2×4) regime in order to maintain smooth surface morphology.

Figure 3 shows the TDD, as measured by planar-view transmission electron microscopy (PVTEM), of numerous $InAs_xP_{1-x}$/InP $(x = 0.5–0.8)$ graded buffer samples grown within a (2×4) regime at 460–480 °C. We found that TDD increases linearly with grading rate, as predicted by Fitzgerald's dislocation dynamics model.[14] For grading rates $\leq 0.5\%/\mu m$, our TDDs of $2–3 \times 10^6 cm^{-2}$ are similar to the lowest reported values for $InAs_xP_{1-x}$/InP $(x \geq 0.45)$ in the literature $(\sim 1–2 \times 10^6 cm^{-2})$, indicating that, in addition to smooth morphology, our choice of buffer growth conditions yields efficient dislocation glide kinetics.[12,18] A grading rate of $0.5\%/\mu m$ was subsequently employed for the devices reported here. Also, note that other techniques such as etch-pit density (EPD) have been attempted for metamorphic InAsP to survey TDD over a wider area. However, EPD was found to underestimate the TDD values by a factor of 10× for $InAs_{0.4}P_{0.6}$,[12] and was not attempted here.

The LED samples were fabricated by first lithographically patterning and wet-etching $500\,\mu m \times 600\,\mu m$ mesas with heights of $1\,\mu m$. Following the mesa etch, metal contacts (Ti:Au = 20 nm:200 nm) consisting of a large-area bonding pad and a gridded region for surface light emission were deposited upon the top of the mesas (p-contact) using a standard UV lithography, metallization, and lift-off process. Contacts to the etched surface surrounding the mesas were made to act simultaneously as n-contacts. Following metallization, the processed chips were mounted on a copper block and wire-bonded. Samples were mounted in a continuous flow vacuum cryostat for the emission measurements. PL measurements were taken using a 532 nm solid-state diode-pumped laser (50 mW), chopped at a frequency of 998 Hz, as the excitation source. The incident laser is focused onto the sample through a quartz window at an angle of 45° to the sample normal, and the PL, emitted through the cryostat's ZnSe window, was collected and collimated by a germanium lens, which also served to prevent the exciting laser light from entering the Fourier transform IR (FTIR). Spectra were collected with a Bruker v80v FTIR spectrometer operating in amplitude modulation step scan mode. The emitted light was detected by the FTIR's internal HgCdTe (MCT) detector and filtered using a lock-in amplifier, whose DC output signal was then sent back into the FTIR. The EL measurement was taken using the same experimental setup, except with the sample electrically excited using an Agilent 33220A function generator. EL and PL spectra were collected as a function of sample temperature, as well as electrical and optical pumping power.

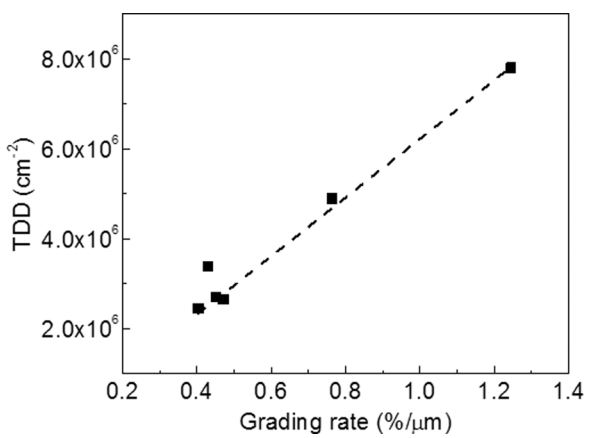

FIG. 3. TDD variation for $InAs_xP_{1-x}$/InP graded buffers $(x = 0.5–0.8)$ as a function of grading rate. Growth rate is $1\,\mu m/h$ and substrate temperature is 460–480 °C for all samples. The dotted line shows linear correlation between TDD and grading rate.

III. RESULTS AND DISCUSSION

Misfit dislocations (MDs) in QWs due to strain relaxation can significantly degrade quantum efficiency, and therefore growing dislocation-free, fully strained InAs QWs is important for the LEDs presented here. Critical thickness calculations were performed using the standard expression,[19] and mechanical constants of the materials were adopted from literature.[20] The theoretical calculations show that the InAs QWs have critical thicknesses of 8.5 and 18.0 nm for sample A and sample B, respectively. We therefore grew a 6 nm QW for sample A and a 10 nm QW for sample B to avoid any strain relaxation. However, cross-sectional transmission electron microscopy (X-TEM) revealed MDs with spacing of $\sim 1\,\mu m$ in the QW interface of sample A [Fig. 4(a)], corresponding to a low strain relaxation of ~1%; no dislocations were observed at the QW interface in sample B [Fig. 4(c)]. The unexpected observation of a sparse array of MDs in sample A emphasizes the need to experimentally calibrate QW critical thicknesses for each QW/barrier composition. To kinetically suppress the formation of MDs, sample A was grown a second time with the substrate temperature lowered to 420 °C prior to the growth of the n-$InAs_{0.51}P_{0.49}$

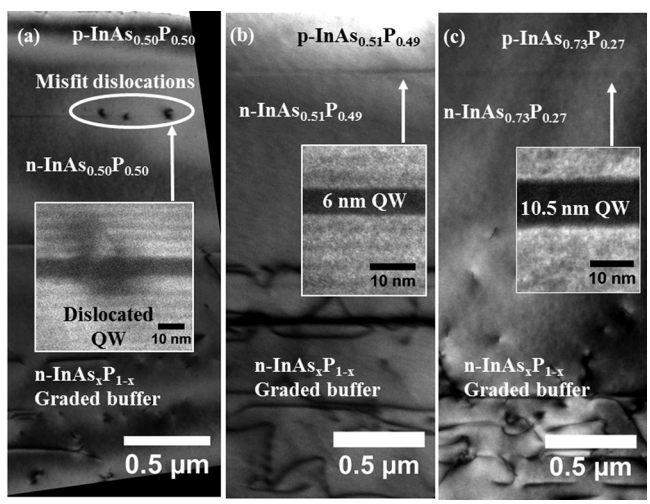

FIG. 4. g = (220) cross-sectional TEM images of (a) sample A grown at 470 °C, (b) sample A with QW grown at 420 °C, and (c) sample B. The insets show InAs QWs under g = (004). Misfit dislocations were observed from sample A grown at 470 °C, while coherent interfaces were found in both sample A grown at 420 °C and sample B.

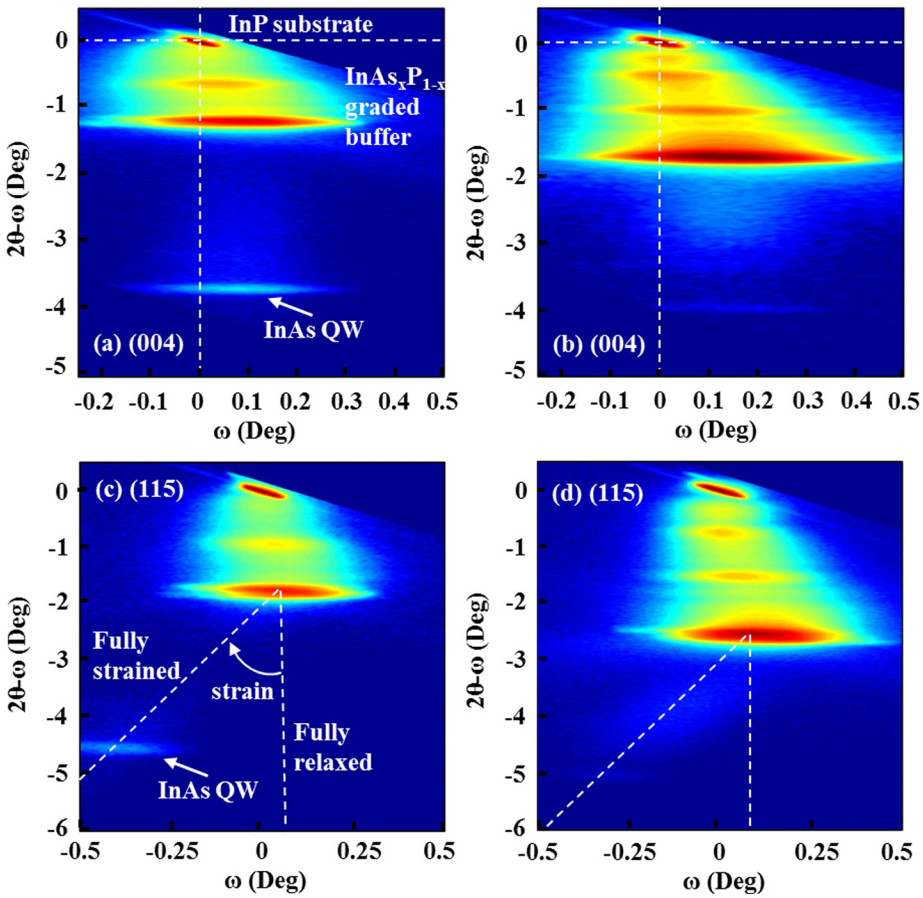

FIG. 5. Reciprocal space map (RSM) of sample A (a) symmetric (004) and (c) asymmetric (115), and sample B (b) symmetric (004) and (d) asymmetric (115). Diffraction intensity from the substrate and graded buffer are visible in the top and middle of the maps. The thin InAs QW appears more faintly below the graded buffer peaks in the (004) RSMs and below and to the left in (115) RSMs due to strain.

barriers and InAs QW.[21,22] The As_2 sticking coefficient at 420 °C is higher than at 470 °C,[23] and the corresponding As_2/P_2 flux had to be adjusted for the designed barrier compositions in sample A. X-TEM images of the regrown sample A [Fig. 4(b)] show the upper portion of the n-type graded buffers and the InAs QW/$InAs_xP_{1-x}$ barriers, revealing smooth and fully coherent interfaces between the QW and the barriers. The measured QW thicknesses are 6 nm and 10.5 nm as shown in the insets of Figure 4.

We conducted high-resolution x-ray diffraction (HRXRD) measurements of the LED samples using a Rigaku Smartlab system to study the relaxation state, composition, and tilt of the $InAs_xP_{1-x}$ and InAs QW layers. Figure 5 shows reciprocal space maps for (004) and (115) glancing incidence reflections. The symmetric (004) scans in Figures 5(a) and 5(b) clearly reveal the entire sample structure, including the InP substrate, $InAs_xP_{1-x}$ graded buffer, and the InAs QW. The cap compositions of sample A and sample B are 51% and 73% with relaxations of 93% and 96%, respectively. In contrast, the InAs QW layers are both fully strained as seen in Figures 5(c) and 5(d). The InAs QW HRXRD peak shows narrower FWHM and higher intensity in sample A than in sample B, despite the thinner QW in sample A and the fact that both QWs were found to be fully coherent in XTEM. The smaller HRXRD FWHM indicates that the QW in sample A is of higher structural quality,[24] as will be discussed in the context of EL and PL results below.

At 77 K, both LED samples show very narrow EL linewidths with the FWHM values of 10 meV and 4 meV for sample A and sample B, respectively (Fig. 6). The larger FWHM in sample A may be caused by its thinner QW and stronger inhomogeneous broadening due to interface

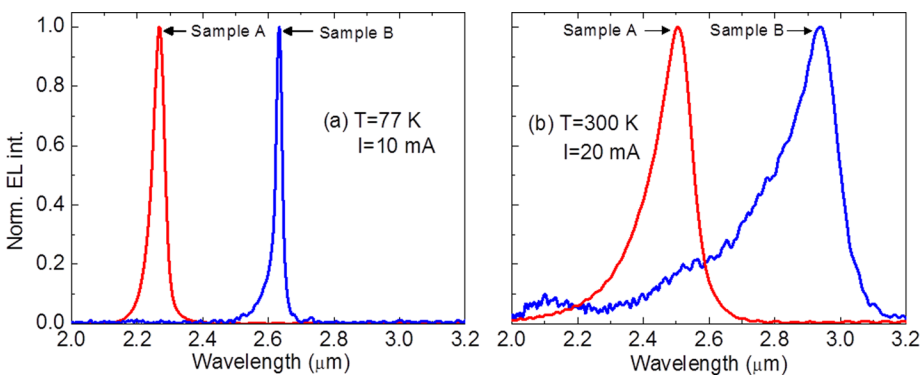

FIG. 6. Electroluminescence spectra of sample A and sample B at (a) 77 K and (b) 300 K.

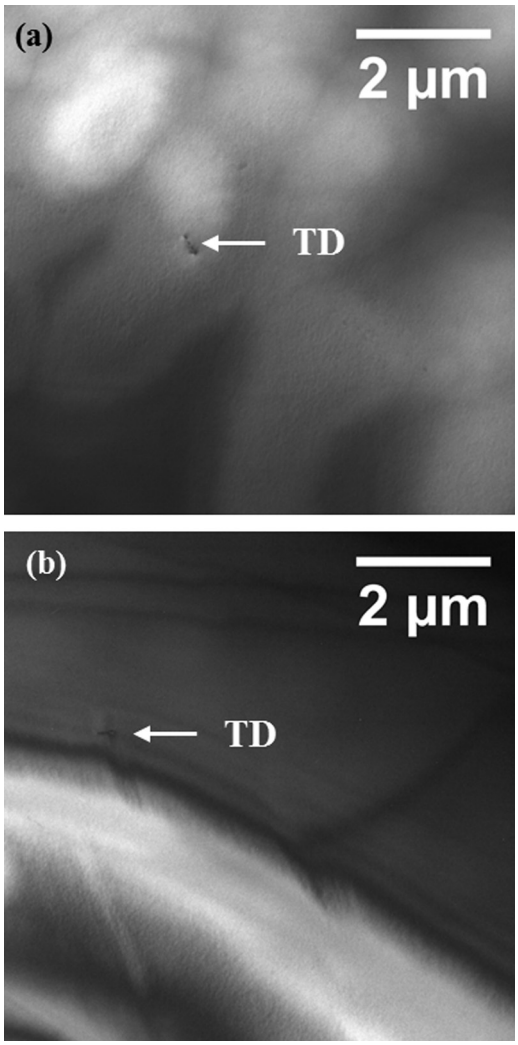

FIG. 7. $7.6 \times 7.6\,\mu m^2$ plan-view TEM images of (a) sample A and (b) sample B p-$InAs_xP_{1-x}$ cap layer under g = (220). TDD values are $2.5 \times 10^6\,cm^{-2}$ and $1.9 \times 10^6\,cm^{-2}$ for sample A and sample B, respectively.

roughness.[25,26] At 300 K, the EL spectra red-shifted from 2.27 μm to 2.50 μm and from 2.63 μm to 2.94 μm for samples A and B, respectively [Fig. 6(b)]. The FWHM of sample A remained relatively small at 22 meV, while the FWHM of sample B increased to 30 meV. Comparing the two LEDs in terms of 77 K EL intensities, sample A exhibited ~16× higher EL intensity than sample B at a forward bias of 10 mA. Our electroluminescence setup is not specifically designed to measure optical output power, and therefore, calculating the internal quantum efficiency of the samples is difficult and remains for future work.[27]

We investigated TDDs by plan-view TEM (PV-TEM) on both samples in an attempt to elucidate the EL intensity disparity in the LEDs. Figures 7(a) and 7(b) show representative $7.6 \times 7.6\,\mu m^2$ PV-TEM images for each sample, showing a single threading dislocation each. We found that both samples A and B had very similar TDDs of $2.5 \times 10^6\,cm^{-2}$ and $1.9 \times 10^6\,cm^{-2}$, respectively, as expected for a grading rate of 0.5%/μm (Fig. 3). Thus, a difference in TDD cannot explain the difference in the EL intensity.

The InAs QW growth temperature may be one of the factors in explaining the intensity disparity.[5,21,22] As noted above, the diffraction intensity from the 6 nm QW in sample A was unexpectedly stronger than that of the 10 nm QW in sample B. Recall also that the QW in sample A was grown at a reduced temperature of 420 °C to suppress dislocation glide, while the QW in sample B was grown at the graded buffer growth temperature of 470 °C. Previous scanning tunneling microscopy studies showed that the density of atomic-scale defects in the InAs homo-epitaxial layers decreases as growth temperature is lowered.[28] Since both PV and XTEM results show that the two samples are very similar in terms of dislocation density, we speculate that the lower InAs QW growth temperature may reduce point defect incorporation, leading to brighter EL and narrower FWHM in HRXRD.

We also studied T-dependent EL, and Figure 8(a) shows that sample A undergoes much less thermal quenching than sample B. From 77 K to 300 K, the integrated EL intensity of sample A drops by a factor of 10, while sample B decreases by a factor of 50. We also carried out T-dependent PL experiments under constant optical excitation (laser power = 50 mW) to investigate the thermal quenching. A similar trend was observed from the T-dependent PL measurement, as shown in Figure 8(b). Note that the thermal quenching from sample A is comparable to W-type mid-IR materials on InP, such as InGaAs/GaAsSb by Pan *et al.*[29] and InAs/InGaSb/AlAsSb by Canedy *et al.*,[30] both of which showed one order of magnitude drop in integrated PL intensity from 77 K to 300 K. This proves that sample A can effectively confine carriers into the QWs by minimizing carrier escape to the barriers at 300 K.

We performed QW energy level calculations for both samples at 300 K using band parameters from the literature[20] to understand the different thermal quenching between the samples. Reported values for the valence band offset ΔE_v

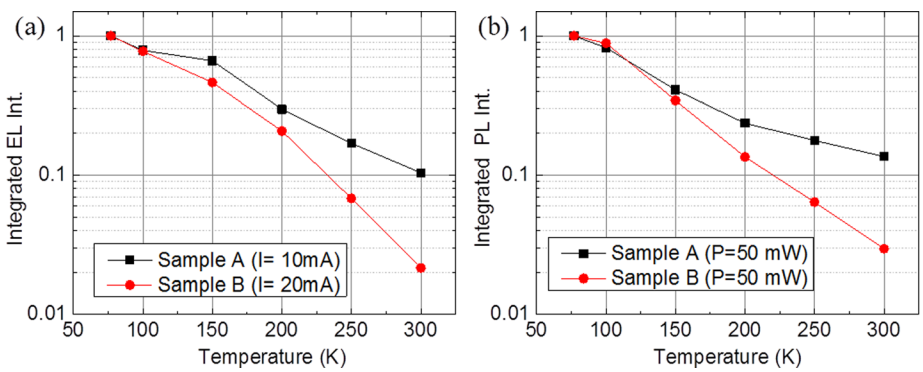

FIG. 8. (a) Integrated EL intensity and (b) integrated PL intensity of sample A and sample B. Both EL and PL reveal that sample B undergoes stronger thermal quenching than sample A.

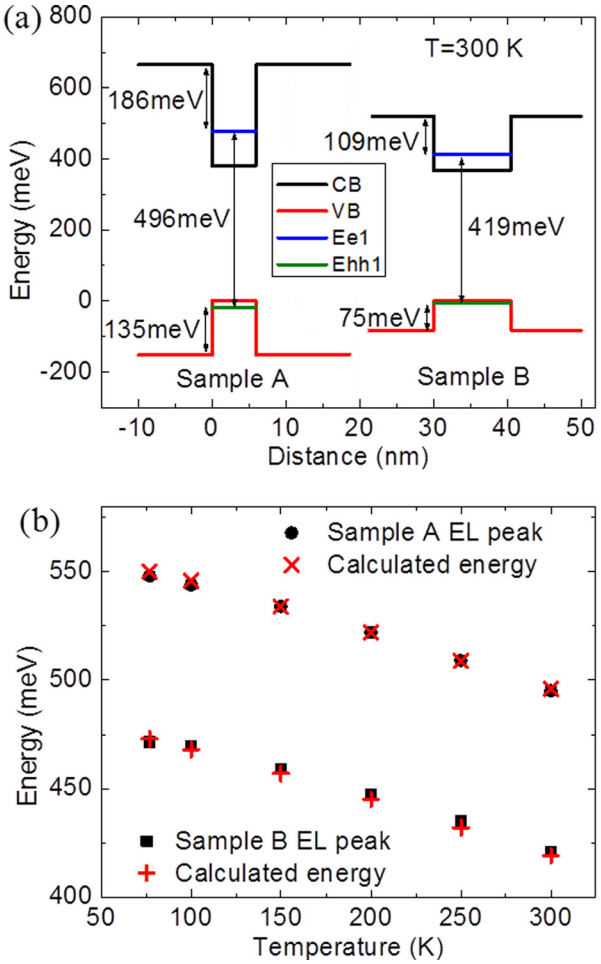

FIG. 9. (a) Calculated QW energy band alignment of sample A and sample B at 300 K and (b) T-dependent EL results showing experimental peak energies (black points) and calculated peak energies (red cross and red x).

between InAs and InP have varied,[31] but we found $\Delta E_v = 0.35\Delta E_g$ to give the best fit to the 300 K EL peak wavelengths for both samples. The energy band-alignments shown in Figure 9(a) illustrate that sample A possesses better carrier confinement for both electrons and holes in the QW than sample B, which can better prevent thermal escape from the QW at RT; the potential barrier for the conduction band of sample A is 77 meV higher than that of sample B, while the valence band barrier is 60 meV higher. Excited states for electrons and holes are omitted for clarity in Figure 9(a). Figure 9(b) shows how the EL peak wavelengths for both samples evolve from 77 K to 300 K, closely matching our calculated transition energies. This indicates an accurate choice of the material parameters and band offsets ($\Delta E_v = 0.35$) over a wide range of InAs QW strains and barrier compositions, enabling us to design and grow the active regions as desired.

IV. CONCLUSIONS

In conclusion, we have described the growth and fabrication of InP-based mid-IR LEDs employing compressively strained InAs QWs on top of $InAs_xP_{1-x}$ metamorphic buffers. A wide range of $InAs_xP_{1-x}$ buffer/barrier compositions could be grown with low TDD as long as a low strain gradient was employed and growth was maintained within a (2×4) regime. The freedom to engineer the bandgap and lattice constant of the barrier layers combined with kinetic suppression of strain relaxation in the InAs QW allowed great design flexibility for mid-IR type-I LEDs. We also found that InAs QW LEDs grown at a lower substrate temperature with 1.53% strain exhibited 16× higher EL intensity and 5× smaller thermal quenching than LEDs grown at higher temperature with 0.84% strain. These encouraging EL results show the potential of InP-based type-I light emitters covering the wavelength gap from $\lambda = 2.4$ to 3.0 μm. For future work on InP-based type-I laser diodes, we speculate that the graded $InAs_xP_{1-x}$ buffer can serve as a graded-index lower cladding layer. Lattice-mismatched upper cladding layers with large index contrast (e.g., AlGaAs) can then be grown on top of the cap layers for optical confinement, as was previously shown for InP-based vertical cavity surface emitting lasers.[32]

ACKNOWLEDGMENTS

D.J. and M.L.L. gratefully acknowledge the funding from Toyota Motor Corporation. Also, D.W. and L.Y. are grateful for the support from the NSF ECCS CAREER Award No. 1157933. Materials characterization facilities used in this work were supported by the Yale Institute for Nanoscience and Quantum Engineering and National Science Foundation MRSEC DMR 1119826.

[1]F. K. Tittel, D. Richter, and A. Fried, Top. Appl. Phys. **89**, 445 (2003).
[2]G. Belenky, L. Shterengas, G. Kipshidze, and T. Hosoda, IEEE J. Sel. Top. Quantum Electron. **17**, 1426 (2011).
[3]K. Vizbaras and M. C. Amann, Semicond. Sci. Technol. **27**, 032001 (2012).
[4]I. Vurgaftman, W. W. Bewley, C. L. Canedy, C. S. Kim, M. Kim, C. D. Merritt, J. Abell, and J. R. Meyer, IEEE J. Sel. Top. Quantum Electron. **19**, 1200210 (2013).
[5]T. Sato, M. Mitsuhara, T. Kakitsuka, T. Fujisawa, and Y. Kondo, IEEE J. Sel. Top. Quantum Electron. **14**, 992 (2008).
[6]Y. Gu, Y. G. Zhang, Y. Y. Cao, L. Zhou, X. Y. Chen, H. Li, and S. P. Xi, Appl. Phys. Express **7**, 032701 (2014).
[7]S. Sprengel, C. Grasse, P. Wiecha, A. Andrejew, T. Gruendl, G. Boehm, R. Meyer, and M. C. Amann, IEEE J. Sel. Top. Quantum Electron. **19**, 1900909 (2013).
[8]N. Bandyopadhyay, Y. Bai, S. Tsao, S. Nida, S. Slivken, and M. Razeghi, Appl. Phys. Lett. **101**, 241110 (2012).
[9]M. Razeghi, N. Bandyopadhyay, Y. B. Bai, Q. Y. Lu, and S. Slivken, Opt. Mater. Express **3**, 1872 (2013).
[10]Y. Gu, Y. G. Zhang, Y. J. Ma, L. Zhou, X. Y. Chen, S. P. Xi, and B. Du, Appl. Phys. Lett. **106**, 121102 (2015).
[11]Y. Y. Cao, Y. G. Zhang, Y. Gu, X. Y. Chen, L. Zhou, and H. Li, Appl. Phys. Lett. **102**, 201111 (2013).
[12]M. K. Hudait, Y. Lin, M. N. Palmisiano, C. Tivarus, J. P. Pelz, and S. A. Ringel, J. Appl. Phys. **95**, 3952 (2004).
[13]D. Jung, Y. C. Song, L. Yu, D. Wasserman, and M. L. Lee, Appl. Phys. Lett. **101**, 251107 (2012).
[14]E. A. Fitzgerald, A. Y. Kim, M. T. Currie, T. A. Langdo, G. Taraschi, and M. T. Bulsara, Mater. Sci. Eng. B-Solid State Mater. Adv. Technol. **67**, 53 (1999).
[15]J. B. Babu and K. Yoh, Appl. Phys. Lett. **97**, 072102 (2010).
[16]R. Contreras-Guerrero, S. Wang, M. Edirisooriya, W. Priyantha, J. S. Rojas-Ramirez, K. Bhuwalka, G. Doornbos, M. Holland, R. Oxland, G. Vellianitis, M. Van Dal, B. Duriez, M. Passlack, C. H. Diaz, and R. Droopad, J. Cryst. Growth **378**, 117 (2013).
[17]H. Ye, L. Li, R. T. Hinkey, R. Q. Yang, T. D. Mishima, J. C. Keay, M. B. Santos, and M. B. Johnson, J. Vacuum Sci. Technol. B **31**, 03C135 (2013).

[18]A. Jandl, M. T. Bulsara, and E. A. Fitzgerald, J. Appl. Phys. **115**, 153503 (2014).
[19]E. A. Fitzgerald, Mater. Sci. Rep. **7**, 87 (1991).
[20]I. Vurgaftman, J. R. Meyer, and L. R. Ram-Mohan, J. Appl. Phys. **89**, 5815 (2001).
[21]E. Tournie, K. H. Ploog, and C. Alibert, Appl. Phys. Lett. **61**, 2808 (1992).
[22]J. S. Wang, H. H. Lin, and L. W. Sung, IEEE J. Quantum Electron. **34**, 1959 (1998).
[23]B. W. Liang and C. W. Tu, J. Appl. Phys. **74**, 255 (1993).
[24]X. Liu, H. Jiang, G. Q. Miao, H. Song, L. Z. Cao, Z. M. Li, and D. B. Li, J. Alloys Compd. **506**, 530 (2010).
[25]C. Weisbuch, R. Dingle, A. C. Gossard, and W. Wiegmann, Solid State Commun. **38**, 709 (1981).
[26]J. Singh, K. K. Bajaj, and S. Chaudhuri, Appl. Phys. Lett. **44**, 805 (1984).
[27]E. Matioli and C. Weisbuch, J. Appl. Phys. **109**, 073114 (2011).
[28]G. R. Bell, M. Itoh, T. S. Jones, B. A. Joyce, and D. D. Vvedensky, Surf. Sci. **433**, 455 (1999).
[29]C. H. Pan, S. D. Lin, and C. P. Lee, J. Appl. Phys. **108**, 103105 (2010).
[30]C. L. Canedy, W. W. Bewley, C. S. Kim, M. Kim, I. Vurgaftman, and J. R. Meyer, J. Appl. Phys. **94**, 1347 (2003).
[31]R. P. Schneider and B. W. Wessels, J. Appl. Phys. **70**, 405 (1991).
[32]L. Goldstein, C. Fortin, C. Starck, A. Plais, J. Jacquet, J. Boucart, A. Rocher, and C. Poussou, Electron. Lett. **34**, 268 (1998).